2020

Hybrid Perovskites with Larger Organic Cations Reveal Autocatalytic Degradation Kinetics and Increased Stability under Light

Dhandapani Venkataraman

Hybrid Perovskites with Larger Organic Cations Reveal Autocatalytic Degradation Kinetics and Increased Stability under Light

Christie L.C. Ellis, Hamza Javaid,[a] Emily C. Smith,[a] D. Venkataraman*

University of Massachusetts Amherst, Department of Chemistry, 690 N Pleasant St, Amherst, MA, 01003

ABSTRACT: Hybrid organic-inorganic perovskites have shown incredible promise as active materials for photovoltaic devices, but their instability to light remains a significant roadblock in realizing these applications. Changing the organic cation has been shown to affect light-induced degradation. As a strategy for increasing the stability of these materials, we replaced varying percentages of methylammonium ion in the archetypical methylammonium lead iodide ($MAPbI_3$) hybrid organic-inorganic perovskite with three significantly larger organic ammonium cations: imidazolium, dimethylammonium, and guanidinium. We were able to synthesize hybrid organic-inorganic perovskites with the same 3D perovskite structure as $MAPbI_3$ with substitution of the larger ions as high as 20-30%. These substituted hybrid organic-inorganic perovskites retained similar optoelectronic properties. We discovered that the light-induced degradation in $MAPbI_3$ and the substituted derivatives are autocatalytic, and we calculated rate coefficients for the degradation. All of the substituted hybrid organic-inorganic perovskites showed slower light-induced degradation compared to $MAPbI_3$ — up to a 62% decrease in degradation rate coefficient — at all substitution percentages up to 20%. This work provides evidence that a high percentage of a variety of large ammonium cations can be substituted into the hybrid organic-inorganic perovskite lattice without compromising its desirable optoelectronic properties. Insight into the autocatalytic mechanism of light-induced degradation will be valuable for designing additional strategies to improve the stability of hybrid organic-inorganic perovskites. We also offer insights into how factors other than size, such as hydrogen bonding, influence the stability of the materials. Overall, we have shown that substitution of methylammonium ion for the much larger imidazolium, dimethylammonium, and guanidinium cations in $MAPbI_3$ is a valid strategy for creating stable hybrid organic-inorganic perovskite derivatives by slowing the rate of light-induced degradation.

INTRODUCTION

Hybrid organic-inorganic perovskites are a promising class of materials for a plethora of electronic and optoelectronic applications.[1-4] Photovoltaics is one of the most prominent applications, as the power conversion efficiencies of hybrid organic-inorganic perovskite photovoltaics have skyrocketed to match or surpass those of current commercial technologies in just a few years.[5] The current record efficiency for hybrid organic-inorganic perovskites photovoltaics is 25.2%, and efficiencies of 29.1% have been reached using tandem hybrid organic-inorganic perovskites -silicon tandem photovoltaics.[6, 7] Hybrid organic-inorganic perovskite photovoltaic devices can be made thin, lightweight, flexible, and semi-transparent using low-temperature, solution-based, scalable fabrication methods, all while maintaining their high efficiencies.

One of the significant roadblocks to commercializing hybrid organic-inorganic perovskites photovoltaics is their instability to operational conditions, such as heat, humidity, applied electrical bias, and light.[8-11] Stability under light is a crucial problem that we need to solve, as light exposure is by definition required for photovoltaic devices. Understanding how hybrid organic-inorganic perovskites degrade under light has not been straightforward.[12, 13] Many experimental techniques used to probe their structure and properties cannot be performed under light. Even when a technique allows for light exposure, it has become apparent that multiple structural and optoelectronic changes take place at a variety of time scales under light, causing samples to change over the course of the measurement.[14, 15] As a result, there are major inconsistencies in the long-term stability data.[16]

At present, there are many proposed hypotheses on how light causes hybrid organic-inorganic perovskite degradation, resulting in widely varied and often contradictory conclusions. For example, the formation of electronic trap states under illumination has been proposed via a variety of mechanisms.[17, 18] Another proposed hypothesis is that degradation may occur via photochemical reactions, either within the hybrid organic-inorganic perovskite active material itself via deprotonation or decomposition of the cation, or with interfacial materials.[19-23] It has been proposed that light can activate the transport of halide ions and/or organic cations.[24-28] Explanations of the effects of this ion migration on degradation are also varied, from the creation of deep trap states at ionic vacancy sites or ionic double layers at interfaces to structural destabilization.[29-31] For example, in mixed halide systems, ion migration has been shown to give rise to photoinduced anionic phase segregation, which alters the stability of the system.[32, 33] Some studies invoke the necessity of a combination of factors for the degradation to occur, such as heat plus light, water plus light, or oxygen plus light.[18, 24, 27, 34-37] In several studies, hybrid organic-inorganic perovskites with the formamidinium cation substituted for the methylammonium ion in the A-site of the lattice have increased light stability.[24, 38-40] However, there is a similar debate around the exact mechanism by which the formamidinium ion increases the stability. It is larger than methylammonium ion, has a much smaller (near zero) dipole moment, and two amine

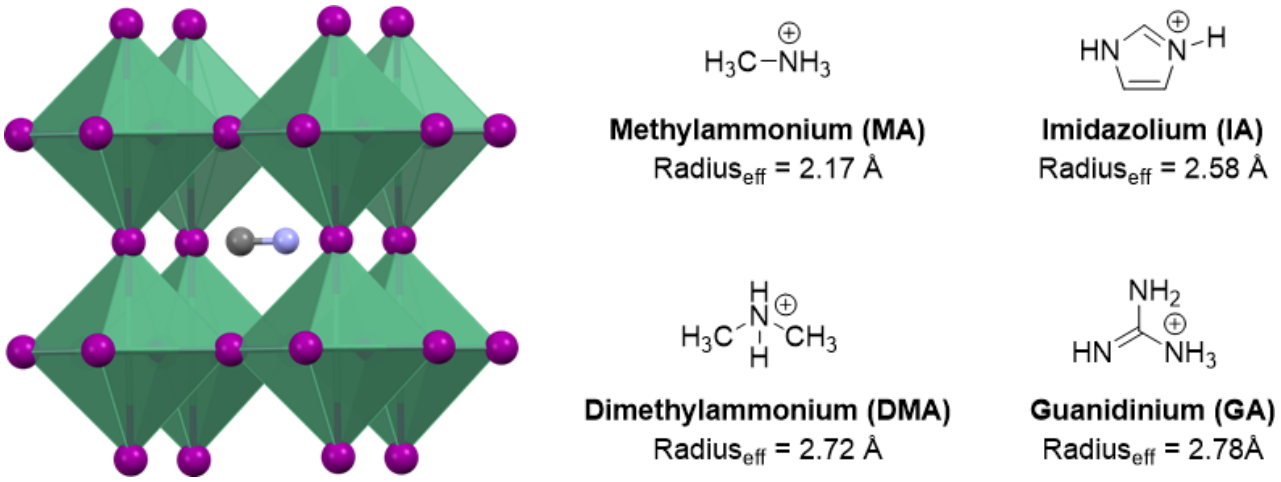

Figure 1. Left: Ideal 3D cubic perovskite structure with ABX_3 stoichiometry, where A is an organic cation (blue-black ion in center of connected octahedra), B is a divalent metal cation (green ion in center of octahedra), and X is a halide anion (purple spheres on corners of octahedra). The archetypical hybrid organic-inorganic perovskite photovoltaic material methylammonium lead iodide ($MAPbI_3$) was used as a starting material for this work. $MAPbI_3$ has a slightly distorted tetragonal structure similar to the cubic structure shown here. Right: Organic ammonium cations used in this work. The larger imidazolium (IA), dimethylammonium (DMA), and guanidinium (GA) ions were used to replace the methylammonium (MA) ion as a strategy for increasing stability of these hybrid organic-inorganic perovskite materials under light.

groups capable of hydrogen bonding as opposed to the single amine group present on the methylammonium ion. These factors affect the structure and electronics of mixed $MA_xFA_{1-x}PbI_3$ perovskites and have also been proposed to slow or stop light-induced ion transport.[29] Overall, there is a clear need for systematic studies investigating the complex interaction between light and hybrid organic-inorganic perovskite materials.

In this work, we show that the light-induced degradation for $MAPbI_3$ and A-site cation substituted derivatives are autocatalytic. We calculated rate coefficients for the degradation and found that partial substitution of methylammonium cation with imidazolium, dimethylammonium, and guanidinium ions slows the light-induced degradation. The maximum decrease in rate was observed in the 5% guanidinium-substituted sample, which degraded 63% slower than $MAPbI_3$. Although all three large ions slowed the degradation, the decrease in rate did not correlate directly with size, suggesting that other factors such as hydrogen bonding may contribute to the increased stability. Our results validate the substitution of all three large ions as a promising strategy for significantly increasing the stability of hybrid organic-inorganic perovskites under light. Direct comparison of these three different ions as a function of both size and substitution percentage allows us to identify trends that may point towards the mechanism of this increased stability. They also provide insight into the autocatalytic mechanism of this degradation reaction, which will aid in design strategies to overcome the crucial stability roadblock.

EXPERIMENTAL SECTION

Lead(II) iodide (PbI_2) (99.9985%) was purchased from Alfa Aesar. Methylammonium iodide (MAI), imidazolium iodide, dimethylammonium iodide, and guanidinium iodide were purchased from GreatCell Solar. Poly(3,4-ethylenedioxythiophene) polystyrene-sulfonate (PEDOT:PSS, Al4083) was purchased from Ossilla. All chemicals were used as purchased.

Glass substrates were cleaned by sonicating 20 min each in deionized (DI) water with detergent, DI water, acetone, and isopropanol, then drying at 150 °C for at least 2 h. The PEDOT:PSS underlayer was coated on glass substrates by treating substrates with UV-O_3 for 20 min, then spin-coating PEDOT:PSS solution filtered through 0.45 µm polytetrafluoroethylene filter onto the substrate at 2500 rpm for 40 s. PEDOT:PSS was then annealed at 150 °C for 30 min.

1.5 M solutions of 1:1 (MAI):PbI_2 and 1:1 LAI:PbI_2 (LA = large ammonium ion) in 7:3 gamma-butyrolactone (GBL): dimethyl sulfoxide (DMSO) were prepared in an N_2-filled glovebox and dissolved by stirring overnight in the dark at 60 °C. After the salts completely dissolved, these solutions were mixed in varying ratios to make mixed $MA_{1-x}LA_xPbI_3$ solutions.

Spin-coating was performed in an N_2-filled glovebox. 100 µL of $MA_{1-x}LA_xPbI_3$ solution was coated onto PEDOT:PSS coated glass substrates at 2000 rpm for 80 s, dripping toluene anti-solvent at 40 s. The resulting films were annealed at 100 °C in the dark for 5 min.

UV-vis absorption spectra were measured on thin films from 250 – 1100 nm on a Shimadzu UV-2401PC.

Effective ionic radii of organic molecules were obtained from the literature.[41] Dipole moments were obtained from the literature or calculated using WebMO with a Gaussian Hartree-Fock 6-31G(d) basis set.

Samples were exposed to 5000 K LED light with ~5 Sun intensity for up to 24 h or until complete degradation of 3D perovskite phase occurred (see SI Figure S1). The spectrum of the LED light and the variations in the intensity and temperature are included in SI Figure S2. This high intensity was chosen to accelerate complete light-induced degradation of samples to take place over a 24 h period. Samples were kept in ambient air at 35 °C and 35-45% RH. Dark control samples were kept in the same ambient conditions.

All powder x-ray diffraction (PXRD) measurements were taken on a SmartLab SE powder diffractometer. Data were analyzed using the SmartLab Studio II software to remove background, identify peaks, calculate peak area, assign peaks to tetragonal structure, and calculate lattice parameters and unit cell volume. Lattice parameter refinement was done by the whole powder pattern fitting (WPPF) method.

Degradation kinetics data (PXRD (110) peak area vs. time exposed to light) was fit to the logistical equation described in the text using Origin 2019 to obtain a composite rate coefficient *k*.

RESULTS AND DISCUSSION

Fabrication and Characterization of Substituted hybrid organic-inorganic perovskite Derivatives. The three large ammonium cations that we chose to replace the methylammonium ion (MA, ionic radius = 2.17 Å) in the A-site of the archetypical $MAPbI_3$ were (in order of increasing ionic radius) imidazolium (2.58 Å), dimethylammonium (2.72 Å), and guanidinium (2.78 Å) (Figure 1). We focused on the effect of size, although these ions do differ in other properties such as hydrogen bonding and dipole moment (see SI Figure S3).

In samples prepared from precursor solutions containing two A-site organic cations, PXRD showed peaks that are characteristic of a three-dimensional (3D) tetragonal perovskite structure that is homeotypic with 3D $MAPbI_3$ tetragonal structure, with slight peaks shifts to lower 2θ values (see Figure 2 and SI Figures S4). This peak shift is consistent is a lattice expansion and is expected with the incorporation of ion larger than methylammonium ion at the A-site (see SI Table S1). We also considered the possibility of the formation of a "hollow perovskite" phase, as has been observed on the addition of large ammonium dications such as ethylenediammonium.[42, 43] Indeed, powder x-ray diffraction patterns for "hollow perovskite" are reported to be nearly identical to their parent analogs, making them difficult to distinguish by this technique.[43] However, the introduction of localized lattice disruptions in "hollow perovskites" result in significant metal and halide vacancy defects which alters the band gap of the material.[43] In this work, we do not observe significant alterations in the band gap after the incorporation of larger cations, thus, we conclude the films retain the 3D structure through the addition of larger cations (SI Table S2).

In PXRD, the perovskite films showed preferred orientation along (110) plane, so the (110) peak, which appears at a 2θ value of ~14, was the most intense in the PXRD pattern (SI Figure S4 (top)). This peak was used to track the presence/absence of the 3D mixed perovskite phase, both initially and as these samples degraded. PXRD patterns of $MAPbI_3$ along with samples prepared from precursor solutions containing 10% of imidazolium, dimethylammonium, and guanidinium ions are shown in SI Figure S4.

In samples prepared from precursor solutions containing up to 10% of imidazolium ions, PXRD showed that the 3D perovskite structure was the exclusive crystalline phase, with only small PbI_2 impurity peaks arising from incomplete conversion during fabrication (see SI Figures S5-S7). For samples prepared with more than 10% imidazolium ions in the precursor solution, the 3D perovskite phase was still present alongside lower-dimensional perovskite phases. The 3D phase remained the majority crystalline phase for samples prepared with 30% imidazolium ion in the precursor solution (based on relative peak intensities). Peaks attributable to the 3D phase was observed even in samples prepared from solutions containing 80% imidazolium ions. Samples with 100% of imidazolium ion as the A-site ion showed only peaks in the PXRD that corresponds to the 1D chain perovskite structure, as previously observed in the literature.[44] PXRD patterns of samples with 100% of the A-site cation as imidazolium, dimethylammonium, and guanidinium ions are shown in SI Figures S8 and S9.

In samples prepared from precursor solutions containing a mixture of 85% methylammonium and 15% dimethylammonium ions, PXRD showed peaks attributable exclusively to the 3D perovskite structure. PbI_2 impurity peaks were not observed in the dimethylammonium containing perovskites. For precursor solution compositions containing greater than 15% dimethylammonium ions, the 3D mixed perovskite phase was still present alongside lower-dimensional perovskite phases. The 3D phase remained the majority phase up to compositions containing 20% dimethylammonium ions. The 3D phase remained through compositions containing 80% dimethylammonium ions. PXRD peaks attributable to the 3D phase was not observed in the sample prepared from solutions 90% dimethylammonium ions. The sample with 100% dimethylammonium ion had the 1D chain perovskite structure, as previously observed in literature with a preferred (010) orientation (see SI Figure S8(b)).[45]

In samples prepared from precursor solutions containing a mixture of methylammonium and up to 20% guanidinium ions, PXRD showed peaks attributable exclusively to the 3D perovskite structure with only small PbI_2 impurity peaks coming from incomplete conversion during fabrication. At compositions above 20% guanidinium ions, the 3D mixed perovskite phase was still present alongside other lower-dimensional perovskite phases (see SI Figure S7). The 3D phase remained the majority phase through precursor solution compositions up to 30% guanidinium ion. Some of this 3D phase remained through compositions containing 80% guanidinium ions. PXRD peaks attributable to the 3D phase was not observed in samples from precursor solution compositions with 90% guanidinium ions. The sample with 100% guanidinium ions had 1D and 2D perovskite structures, as previously observed in literature (see SI Figure 9).[46-48]

Photographs of the samples with mixed A-cation compositions are included in SI Figure S10. A majority of the samples have the same black-brown color as the $MAPbI_3$ control, even in compositions with higher percentages of the larger ion where we observed that other phases coexist with the 3D perovskite in PXRD. As the ion substitution increased, the samples have a fainter brown color. The 100% substituted samples were pale yellow for dimethyl ammonium and imidazolium perovskites and bright yellow for the guanidinium perovskite.

The amount of a particular ion that can be incorporated into the lattice before any measurable quantity of secondary phases are formed did not appear to decrease with increasing size. The smallest ion, imidazolium, formed 3D perovskite up to 10% incorporation whereas the largest ion, guanidinium, formed primarily 3D perovskite up to 20% incorporation. Dimethylammonium ion, which is of intermediate size, fell in the middle at 15%. However, all three ions showed the homeotypic 3D perovskite phase as the majority phase up to a similar percentage (20% for dimethylammonium, and 30% for guanidinium and imidazolium ions). We surmise that the formation of secondary phases may be more strongly related to the formation energy and stability of these lower-dimensional secondary phases than the instability of the 3D perovskite structure.[44-48]

A comparison of the PXRD patterns of samples containing 0%, 50%, and 100% dimethylammonium ions is shown in SI Figure S11. For samples containing 20-80% of dimethylammonium ions, every peak can be attributed to either the 3D tetragonal perovskite or 1D chain perovskite phase, suggesting these two phases coexist. Perovskite samples containing imidazolium ions also behaved similarly. Guanidinium-containing perovskites, however, have more than one phase present at 100% substitution and have peaks in the mid-range substitution percentages, which cannot be attributed to either the 100% phases or the 3D tetragonal phase.

We also observed shifts of the (110) and (220) peaks to lower 2θ angles in the PXRD patterns of the substituted hybrid organic-inorganic perovskites, indicating an increase in lattice size (Figure 2a). This increase was roughly correlated to size, as larger ions led to a larger shift. Samples containing dimethylammonium ions did show a larger shift at lower substitution percentages (up to 20%) compared to samples with guanidinium ions, but these ions are much more similar in size (0.06 Å difference in ionic radius) than methylammonium or imidazolium is to either of them. Guanidinium-containing perovskites showed a larger shift than dimethylammonium containing perovskites at substitution percentages of over 30%. An example of the (110) peak shift in $MAPbI_3$ and the 20% substituted samples is shown in Figure 2. The peaks shifted further to lower 2θ with increasing substitution percentages for all three ions; the d_{110} versus substitution percentage is shown in Figure 2. The spacing between these planes increased with increasing substitution for all three large ions —until ~15-20% incorporation for imidazolium and dimethylammonium and 40% incorporation for guanidinium — at which point it leveled out to a relatively constant value.

The increase in lattice size, which trends with both ionic size and increasing substitution percentage, indicates that the large ions are incorporated into the A-site of the 3D lattice and not merely present in grain boundaries or on the surface. Additionally, the lattice size stays relatively constant even at high substitution percentages where we know that the lower-dimensional perovskite phases coexist with the 3D perovskite phase. This indicates that larger ions are not excluded in favor of a mixed 3D perovskite with lower substitution percentage even when other crystal structure pathways are present for the large cations. Thus, for ensuing discussions, we surmise that a defined fraction of the methylammonium ion has been substituted with the large organic cation.

The lattice parameters and increase in unit cell volume for all substituted compounds up to 20% were calculated based on PXRD data, shown in Figure 2 and detailed in SI Table S1. As

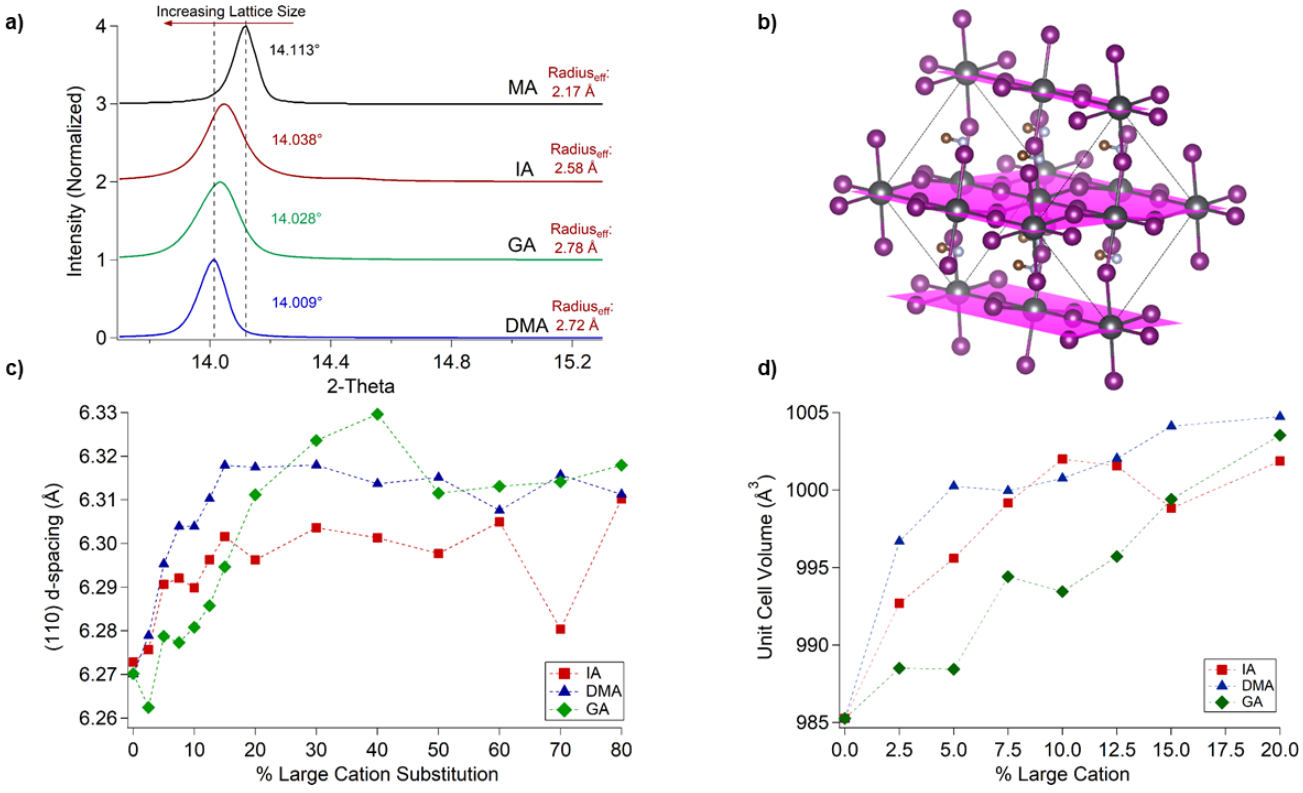

Figure 2. (a) Shift of the (110) peak in $MAPbI_3$ (top) and hybrid organic-inorganic perovskites substituted with 20% imidazolium (IA), guanidinium (GA), and dimethylammonium (DMA). The peak shift to lower angles indicates an increase in lattice size, which generally trends with ionic size. Dimethylammonium (DMA) and guanidinium (GA) are switched as guanidinium (GA) is slightly larger, but the difference in dimethylammonium (DMA) and guanidinium (GA) ionic radii (0.06 Å) is much smaller than the gap between these two ions and methylammonium (MA) or imidazolium (IA) ions. (b) (110) planes in $MAPbI_3$. (c) d-spacing between the (110) planes versus increasing substitution percentages. Spacing between these planes increases along with substitution percentage to a point, after which it levels out. For imidazolium (IA) and dimethylammonium (DMA), this happens at ~15-20%, with the larger dimethylammonium (DMA) settling at a larger d-spacing value than the smaller imidazolium. Guanidinium (GA), the largest ion, starts out with a relatively small d-spacing compared to dimethylammonium (DMA) or imidazolium (IA) but eventually increases to approximately equal to/slightly larger than dimethylammonium (DMA) at ~30%. (d) Increase in unit cell volume with increasing substitution percentage.

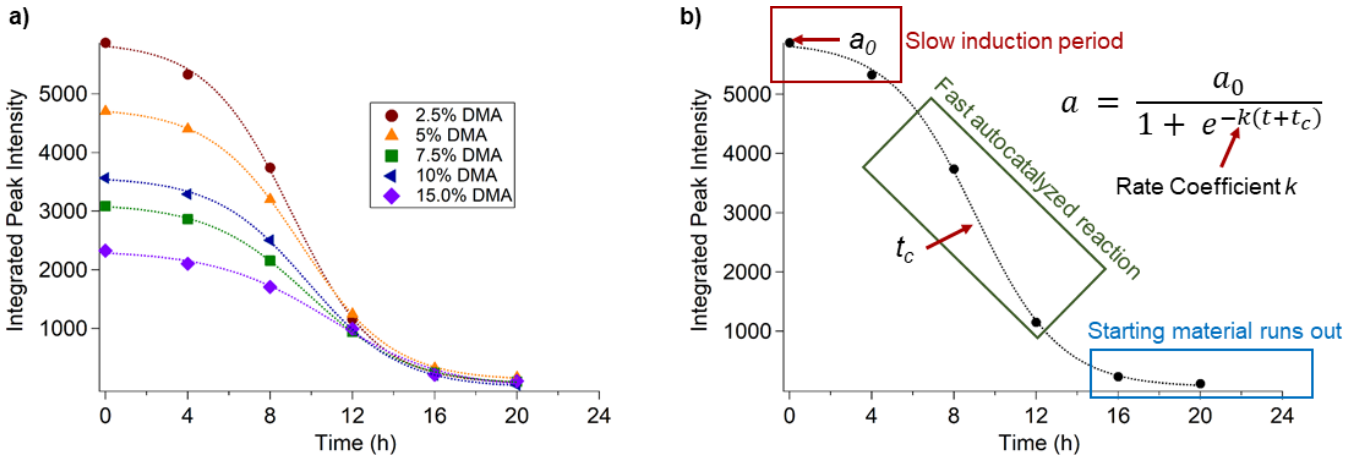

Figure 3. (a) Area of (110) PXRD peak vs time exposed to light for hybrid organic-inorganic perovskites with varying percentages of dimethylammonium (DMA). Hybrid organic-inorganic perovskites substituted with all three ions showed these "S"-shaped curves, indicating an autocatalytic degradation reaction mechanism. (b) Schematic of the phases of the autocatalytic reaction which give rise to the "S'-shaped curves and equation fitting these curves. We extract a rate coefficient k for the degradation reaction from the fitting for each of these samples.

expected from the (110) and (220) peak shifts, the volume of the unit cell increased with increasing substitution percentage to accommodate the larger ions. The trends for dimethylammonium and imidazolium ions seem to correlate to their size, as both increases at similar rates, but imidazolium ion gave a smaller unit cell volume than dimethylammonium ion. Guanidinium ion, however, increased in unit cell volume much more slowly than dimethylammonium or imidazolium ion at low substitution percentages but eventually reached a volume greater than imidazolium and similar to dimethylammonium ion. $MAPbI_3$ gave a unit cell volume of 985 $Å^3$. In samples with 20% of the large cations, we obtained a unit cell volume of 1002 $Å^3$ (1.7% increase) with for imidazolinium, 1004 $Å^3$ (1.7% increase) for guanidinium, and 1005 $Å^3$ (2.3% increase) for dimethylammonium ions. Lattice parameters were only refined up to 20% substitution, but based on the peak shifts for 30-40% guanidinium ion, it is likely that the lattice of guanidinium-based perovskites continues to expand to the largest overall value after dimethylammonium and imidazolium ions volumes become constant.

UV-vis spectra were recorded for all of the substituted compounds up to 20%, and the band gaps were calculated from Tauc plots of this data, shown in SI Figure S12. While the samples showed a slight increase in absorption from 350-550 nm and a slight decrease in absorption from 550-750 nm, the overall absorption profile remained very similar for all substituted compounds. The calculated band gaps varied by <1% for all substituted compounds and did not show any significant trend. The calculated band gaps are listed in SI Table S2. This maintenance of the band gap of $MAPbI_3$ in the substituted hybrid organic-inorganic perovskites, which is well-suited for photovoltaic applications, is promising for the viability of these new compounds.

Light-Induced Degradation Kinetics. We hypothesized that substituting the methylammonium ion in $MAPbI_3$ with larger imidazolium, dimethylammonium, and guanidinium cations would improve the stability of these compounds under light. To test our hypothesis, we exposed the 0-100% substituted thin films to a very bright (~ 5 Sun) LED light for 24 h under ambient conditions and monitored their degradation. The high brightness was chosen in order to (1) accelerate the degradation reaction so that we could observe the entire degradation over the 24 h period and (2) ensure that light was the primary stressor in causing degradation over other environmental factors such as heat or humidity since the experiments were carried out in ambient air. Control samples were kept in the dark in the same ambient conditions as the degraded samples to determine whether other conditions such as temperature or humidity did cause any degradation over the 24 h period. These samples did not show any degradation by PXRD analysis over the 24 h period, indicating that the degradation measured in the primary samples is light-induced (SI Figure S13). Photographs of the samples before and after the 24 h light exposure, as well as the dark control samples, are included in SI Figure S10. After complete degradation, all of the films turned yellow. This color comes from a mix of bright yellow PbI_2, the primary degradation product of $MAPbI_3$, and the lower dimensional perovskites (imidazolium and dimethylammonium lead triodides are pale yellow compounds whereas guanidinium lead triodide is bright yellow). Images of the set-up for the light degradation experiments, the spectrum of the LED light, and the variations in the intensity and temperature over time are included in SI Figures S1and S2. The intensity and temperature were reasonably constant over experiment time.

We used PXRD to track the light-induced degradation of the 3D perovskite structure by measuring the samples every 4 hours through a 24 h period and calculated the decrease in (110) peak area (the most intense peak of the 3D perovskite phase). Using this peak area vs. time data, we were able to rule out simple zero-, first-, and second-order kinetic mechanisms (shown in SI Figure S14). We noticed a characteristic "S"- sigmoidal shape of all of the peak area versus time plots, an example of which is shown in Figure 3.[49-51] This shape is characteristic of an autocatalytic reaction, where one of the reaction products acts as a catalyst to speed up the reaction. Autocatalytic decomposition in solid-state systems can be fit to Equation 2 below[49-51]:

$$a = \frac{a_0}{1 + e^{-k\,(t+t_c)}} \qquad (2)$$

Where a = area of (110) peak, a_0 = area of (110) peak at time zero, k = composite rate coefficient, t = time (hours), and t_c =

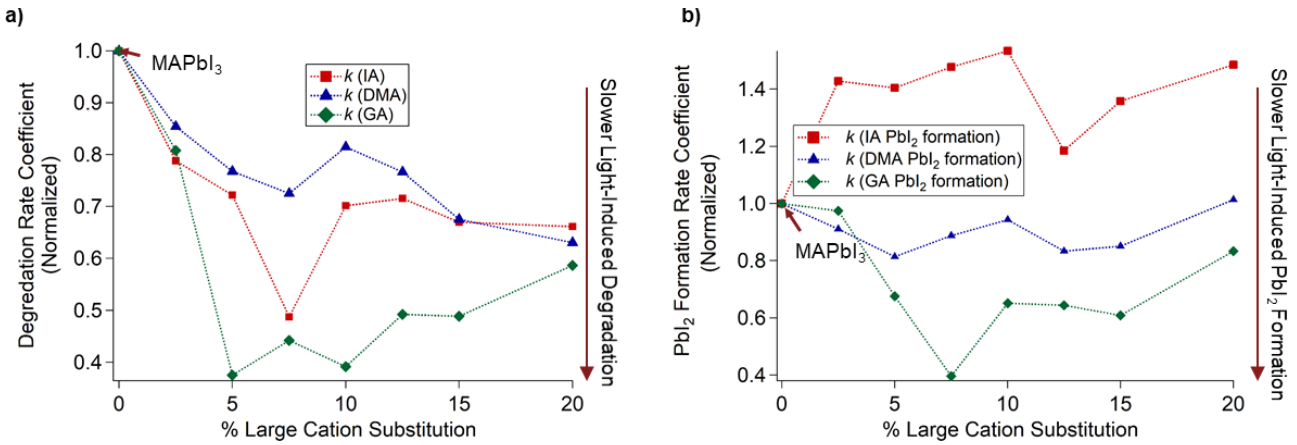

Figure 4. (a) Normalized rate coefficients (k) for the autocatalytic light-induced degradation reaction of the substituted hybrid organic-inorganic perovskites. All three of the ions at every substitution percentage showed slower light-induced degradation than $MAPbI_3$. 5% guanidinium (GA) showed the slowest degradation, a 62.48% decrease in rate coefficient from $MAPbI_3$. (b) Normalized rate coefficients (k) for formation of PbI_2 during the light-induced degradation reaction. Increasing percentages of guanidinium (GA) and dimethylammonium (DMA) formed PbI_2 more slowly than $MAPbI_3$, as expected from their slower degradation. Imidazolium (IA), however, showed faster PbI_2 formation than $MAPbI_3$ despite degrading more slowly.

critical point. Using this to fit our peak area versus time data, we were able to obtain a composite rate coefficient *k* for the light-induced degradation reaction of each of the substituted derivatives. A schematic of how this reaction mechanism and equation lead to the observed "S"-shaped sigmoidal curve is shown in Figure 3. Rate coefficients were only calculated up to 20% substitution, as many of the higher substitution percentages degraded before 24 h and thus had fewer data points. All of the calculated rate coefficients and their percent change compared to $MAPbI_3$ can be found in SI Table S3. This complex rate coefficient may capture more than one degradation pathway, as discussed below, but it offers a useful tool for comparing the relative degradation rate of the materials with one another.

We found that every one of the substituted derivatives up to 20% had a smaller *k* — corresponding to a slower light-induced degradation reaction — compared to $MAPbI_3$. The *k* numbers as a function of large cation substitution percentage normalized to their $MAPbI_3$ control are shown in Figure 4a. All three cations showed a steep initial decrease in *k* from ~0-5% substitution, after which they either leveled out or increased slightly. However, none ever went back up to the level of $MAPbI_3$. Dimethylammonium containing compounds showed the smallest decrease in rate coefficients compared to $MAPbI_3$, with a maximum decrease in *k* of 37% at 20% dimethylammonium substitution. The maximum decrease in *k* for imidazolium containing perovskites was 51% at 7.5% imidazolium substitution. Guanidinium containing perovskites showed the largest decrease in *k* of all of the large cations, with a maximum decrease of 62.48% with 5% guanidinium substitution. Even the smallest decrease in *k* – 14.6% for 2.5% dimethylammonium substitution—represents significantly improved light stability compared to $MAPbI_3$. This is strong evidence supporting our hypothesis that substituting any of the three larger imidazolium, dimethylammonium, and guanidinium cations for methylammonium ions would lead to more stable hybrid organic-inorganic perovskite compounds.

Interestingly, the decrease in *k* did not directly correspond to an increase in ionic size. The largest ion, guanidinium, led to the most stable compounds at nearly all substitution percentages. However, the smallest of the three ions, imidazolium, led to more stable compounds than the larger dimethylammonium ion. This indicates that factors beyond size must be considered in evaluating the impact of new organic cations on stability under light.

Guanidinium-containing perovskites exhibited behavior that deviated from expected size trends both in initial structure and degradation kinetics. Guanidinium ion differs from the other ions in that it has no dipole and has several more potential hydrogen bonding sites.[52] The decrease in *k* did trend with the number of amine functional groups capable of hydrogen bonding. Dimethylammonium (least decrease in *k*) has one, imidazolium (middle) has two, and guanidinium (largest decrease in *k*) has three. Size undoubtedly plays a role, however. Although dimethylammonium and methylammonium ions have the same number of amine functional groups, the amine group on the methylammoninum ion is less sterically hindered; thus, the ammonium group on the methylammonium ion can form stronger hydrogen bonds than dimethylammonium. Therefore, if only hydrogen bonding were responsible for the increase in stability, dimethylammonium substituted compounds would likely be less stable than $MAPbI_3$. The strength of hydrogen bonds in these materials is difficult to quantify,[53] as factors such as geometry, rotational freedom, polarizability, and potential for concerted hydrogen bonding could all play a role.

Since PbI_2 is the primary degradation product of $MAPbI_3$, and we know that the substituted samples degrade more slowly than $MAPbI_3$, we might expect that the rate of PbI_2 formation would decrease with increasing large cation substitution. The rate of PbI_2 formation shown in Figure 4b was calculated based on fitting the area of the (001) peak versus time plot (which showed the same unique S-shape) and is shown as a function of organic cation substitution. This does seem to be the case for dimethylammonium and guanidinium. Both showed slower PbI_2 formation than $MAPbI_3$, and the rate decreased more in guanidinium than dimethylammonium, which was consistent with trends in degradation rate. Samples with imidazolium ions,

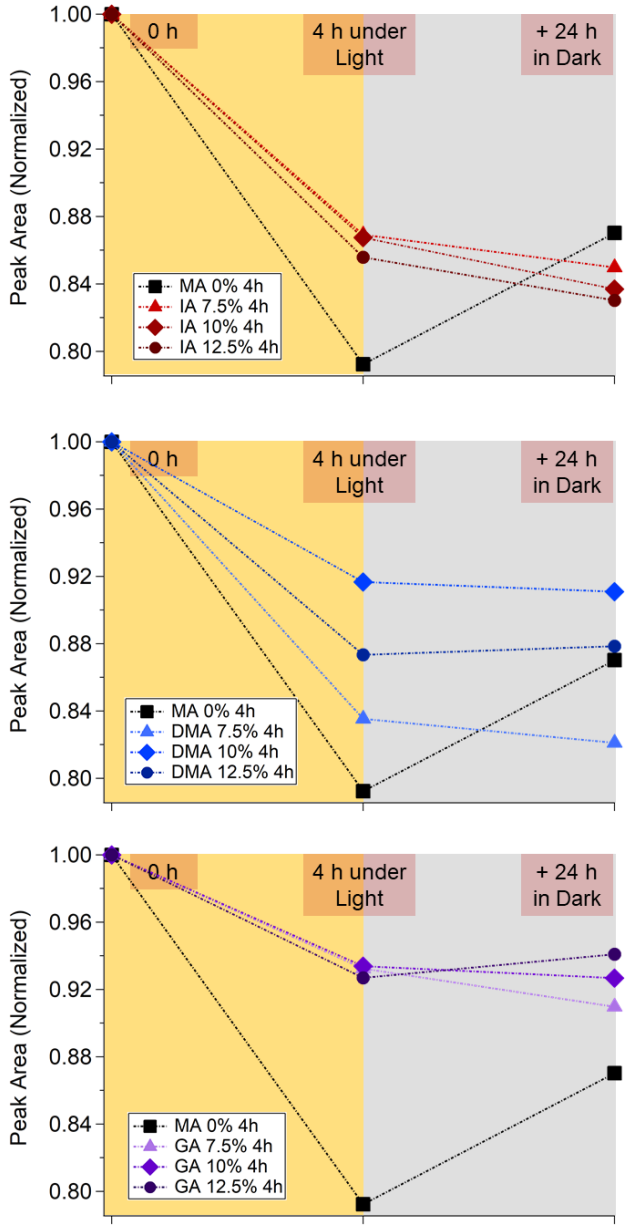

Figure 5. Normalized area of (110) peak in $MAPbI_3$ and hybrid organic-inorganic perovskites substituted with 7.5%, 10%, and 12.5% imidazolium (IA) (a), guanidinium (GA) (b), and dimethylammonium (DMA) (c). The first point is initial value, the second is after 4 h of light-induced degradation, and the third is after 24 h of resting in the dark. $MAPbI_3$ degraded more than any of the substituted samples in 4 h. However, $MAPbI_3$ degradation was partially reversible, while the substituted hybrid organic-inorganic perovskites either stayed the same or degraded slightly more.

however, showed the opposite behavior, with the PbI_2 formation rate increasing as a percentage of imidazolium substitution.

Rate of PbI_2 formation does not give a complete picture of degradation products, however, as alternative lower-dimensional degradation products can also form when these larger cations are introduced. Differences in the formation energy and stability of these alternative products could influence the rates of formation of PbI_2 in addition to the overall degradation rate. We were unable to quantify the rate of formation for these 1D products since for the majority of the lower percent substitution samples, this peak did not appear at all or did not appear until very late in degradation (values listed in SI Table S4). We also note that if amorphous products form during the degradation, then PXRD will not be useful to quantify their rates of formation. General observations point to differences in 1D product formation between the three ions. Additionally, amorphous forms of these materials present in the original sample or as a product of degradation could play a role, which we could not quantify due to the limitations of PXRD. Analysis of the role of these amorphous materials will be the subject of future study.

We observed no evidence of the most intense (110) peak from the 1D imidazolium perovskite phase in imidazolium samples up to 10% substitution. 12.5% - 20% imidazolium substitution had this peak, but its area did not change with time of light exposure and did not strongly correlate to the percent of imidazolium substitution. Samples with 0-15% dimethylammonium ions did not show any evidence of the most intense (010) peak from the 1D dimethylammonium phase, except for a very small peak that appeared at 12-16 h and disappeared at 20 h. Samples containing 20% dimethylammonium ion, however, showed a 1D peak, which degraded with increasing light exposure time. None of the 0-20% guanidinium containing samples showed the most intense (120) 1D guanidinium phase peak at 0 h.[54, 55] The 0-5% guanidinium containing samples never showed this peak through the degradation, but it appeared for the 20% sample at 4 h, the 10, 12.5, and 15% samples at 8 h, and the 7.5% sample at 12 h. Additionally, unlike the 1D peaks in imidazolium or dimethylammonium containing samples, the area of the 1D peaks for all of the guanidium-containing samples increased with both increasing degradation and increased guanidinium substitution percentage. This may point to a lower formation energy of 1D guanidinium degradation products compared to PbI_2, which seems to be favorable given that guanidinium shows the largest increase in stability.[38]

To gain further insight into the mechanism of light-induced degradation, the reversibility of this reaction was investigated. Samples of $MAPbI_3$ and 7.5%, 10%, and 12.5% large cation substituted hybrid organic-inorganic perovskites were measured by PXRD, exposed to light for 4 h and measured again, then placed in the dark for 24 h and measured a final time (Figure 5). After the 4 h light degradation, $MAPbI_3$ (black curve in Figure 5a, b, and c) degraded to 79% of its initial value, significantly more than any of the substituted samples, as expected. After resting for 24 h in the dark, $MAPbI_3$ recovered to 87% of its original value, indicating the partial reversibility of this reaction, as observed in previous studies.[24] However, none of the substituted samples showed any reversibility in their degradation, either staying constant or degrading slightly more. This points to a combination of both reversible and irreversible degradation factors that affect the substituted hybrid organic-inorganic perovskites differently than $MAPbI_3$.

Light-activated ion transport could act as a reversible degradation mechanism.[24, 28, 29, 31, 56] The more stable substituted samples may show less ion migration out of the lattice compared to $MAPbI_3$ because of increased hydrogen bonding with the inorganic lattice, increased steric hindrance for methylammonium ions, increased activation energy for the movement of larger cations, or passivation of grain boundaries as a path for ion movement. However, by the same argument, after the light is turned off, the ions which moved out of the structure may not be able to diffuse back into the structure. This would lead to a

lack of recoverability compared to the smaller, more mobile methylammonium ion in $MAPbI_3$ samples.

Chemical reactions could act as irreversible degradation mechanisms, and, logically, these different molecules would have different reactivities. One study conducted by Pont et al. observed autocatalytic degradation of mixed halide hybrid organic-inorganic perovskites under light in ambient air.[57] They ruled out oxygen diffusion through the film as the cause for the delayed onset of light-induced degradation, instead hypothesizing that one of the degradation reaction products was acting as the catalyst. They noted, however, that films with bromide were much more light-stable than those with iodide. I_2 is a common reactive species invoked in hybrid organic-inorganic perovskites, but there is disagreement on how it is formed and how it reacts.[58-62]

Fu et al. identified an autocatalytic light-induced degradation reaction in $FA_xMA_{1-x}Pb(I_yBr_{1-y})_3$ hybrid organic-inorganic perovskite photovoltaic devices and assigned I_2 as the catalyst in their systems.[62] They observed that their encapsulated devices ruptured from the built-up pressure of I_2 after a certain amount of light-induced degradation, while bare films showed significantly increased stability. They measured the gases which evolved from their system and found I_2 and CH_3I. However, the reaction where I^- displaces NH_3 may not be able to proceed similarly with all the compounds we used in this work. Dimethylammonium ion could potentially react similarly with CH_3NH_2 as the leaving group rather than NH_3. Imidazolium and guanidinium ions, however, are unlikely to react with I^- ions via a substitution reaction.

On the other hand, Wang et al. proposed that I_2 could form $I_2^{\cdot-}$ under light, which would react with $CH_3NH_3^+$ to form CH_3NH_2, I_2, and H_2.[61] All of the species used in this work have protons which could be removed. We examined the pKa values for the ions used in this work. In order from most to least acidic were imidazolium (6.95), methylammonium (10.6), dimethylammonium (10.8), and guanidinium (12.5) ions. This does not exactly follow the degradation trends, as imidazolium substituted samples degrade more slowly than $MAPbI_3$. However, it does trend with the rate of PbI_2 formation, so deprotonation may be involved in the pathway of the degradation reaction, which forms PbI_2 as a product.

Light is a primary driving factor for the accelerated autocatalytic degradation observed across these studies, in hybrid organic-inorganic perovskites with both mixed cations and mixed halides. Fu et al. conducted their work in an N_2 atmosphere under high heat (80 °C) and noted that the degradation would not proceed without light, but that even a low-intensity light would trigger it. Pont et al. observed the same autocatalysis, but at room temperature under ambient conditions with a very low-intensity fluorescent light (~2 mW cm^{-2} intensity at 550 nm). We conducted our studies in ambient air at 35 °C, and 35-45% RH with a very intense LED light and observed this same autocatalytic degradation, and did not observe any degradation under these same conditions in the dark. Therefore, we surmise that the visible light is a necessary factor that initiates autocatalytic decomposition.

The influence of light on hybrid organic-inorganic perovskites that leads to degradation is complex and multifaceted, but the increased stability of these new hybrid organic-inorganic perovskite derivatives substituted with imidazolium, dimethylammonium, and guanidinium ions provides some new insights. There are both reversible and irreversible components to the degradation. The substituted hybrid organic-inorganic perovskites appear to degrade by the irreversible mechanism, but the effects of the reversible mechanism are substantially reduced. Reactive iodide species may be formed under light, and finding organic cations which do not undergo these irreversible reactions – either because of steric hindrance, increased pKa, or different molecular geometries – should increase stability. All of the cations tested here could undergo chemical reactions to some extent, but the low pKa of dimethylammonium and guanidinium ions may be contributing to their increased stability. Chemical reactions do not seem to be the only source of degradation in $MAPbI_3$, however, as a distinct reversibility is observed in these samples which is not present in the substituted derivatives. This reversible degradation seems to be the primary pathway that is avoided in the substituted hybrid organic-inorganic perovskites. Increased activation energy for ion transport with the larger ions may lead to this decrease in reversible light-induced degradation; this will be investigated in future works.

CONCLUSIONS

We successfully fabricated hybrid organic-inorganic perovskites with 0-100% substitution of the methylammonium (MA) cation in archetypical $MAPbI_3$ with the larger imidazolium, dimethylammonium, and guanidinium compounds. These substituted hybrid organic-inorganic perovskites maintained a $MAPbI_3$-like 3D tetragonal perovskite structure as a primary or secondary phase up to high substitution percentages, despite predictions that these cations were too large to fit into the methylammonium ion lattice site. These compounds showed increasing lattice size with increasing substitution percentage as well as with increasing ionic radius, suggesting their integration into the lattice itself. We also do not see any evidence that the largest ion we tested, guanidinium (2.78 Å), represents the upper limit of the size of ion that can be incorporated into the 3D lattice. Therefore, it is possible that ions even larger than guanidinium could be substituted for the methylammonium ion to create new hybrid organic-inorganic perovskite derivatives. The band gaps of these compounds remained constant at the same value as $MAPbI_3$, which is well-suited for the desired photovoltaic applications. After characterizing their degradation under illumination, we found that every one of the hybrid organic-inorganic perovskite derivatives up to 20% substitution showed increased stability compared to $MAPbI_3$, with a maximum decrease in the degradation rate of 62% for 5% guanidinium ion substitution. We observed a unique autocatalytic mechanism of this light-induced degradation, which will provide important insights into further understanding of how these cations improve hybrid organic-inorganic perovskite stability and how to design even more stable materials. We also noted how characteristics of the larger cations other than size, such as dipole and hydrogen bonding, may play a role in stability. This was especially noticeable for guanidinium ion, the only ion with no dipole and three amine sites, which showed noticeable deviations from size trends in both structure and degradation kinetics. Overall, we have confirmed our hypothesis that substitution of imidazolium, dimethylammonium, and guanidinium ion for the methylammonium ion in $MAPbI_3$ hybrid organic-inorganic perovskites yield compounds with improved light stability which are promising alternatives for use in hybrid organic-inorganic perovskite photovoltaic applications.

ASSOCIATED CONTENT

Supporting Information.

The Supporting Information is available free of charge via the Internet at http://pubs.acs.org:

Molecular properties of organic cations tested, PXRD of substituted compounds, pictures of pristine and degraded samples, lattice parameters, experimental set-up, spectrum of light used in degradation experiments, demonstration of lack of fit to simple kinetic models, rate coefficients, peak areas of 1D products

AUTHOR INFORMATION

Corresponding Author

* Email: dv@umass.edu

[a] HJ and ES equally contributed to this work

Funding Sources

We gratefully acknowledge the financial support of the US Army CCDC Solider Center through contract no. W911QY1820002 for this work. The powder X-ray diffractometer used in this study was acquired through the National Science Foundation Major Research Instrumentation Program (NSF CHE-1726578).

ACKNOWLEDGMENTS

We thank Professor Mark Turnbull of Clark University for his help in gathering initial PXRD data of the substituted compounds. We thank Dr. Ravi Mosurkal, Professor Jayant Kumar, Professor Lian Li, and Dr. Youngju Bae of University of Massachusetts Lowell for fruitful discussions.

REFERENCES

(1) Green, M. A.; Ho-Baillie, A.; Snaith, H. J. The emergence of perovskite solar cells. *Nat. Photon.* **2014,** *8*, 506-514.

(2) Jena, A.; Kulkarni, A.; Miyasaka, T. Halide Perovskite Photovoltaics: Background, Status, and Future Prospects. *Chem. Rev.* **2019,** *119*, 3036-3103.

(3) Petrus, M. L.; Schlipf, J.; Li, C.; Gujar, T. P.; Giesbrecht, N.; Müller-Buschbaum, P.; Thelakkat, M.; Bein, T.; Hüttner, S.; Docampo, P. Capturing the Sun: A Review of the Challenges and Perspectives of Perovskite Solar Cells. *Adv. Energy Mater.* **2017,** *7*, 1700264.

(4) Grätzel, M. The light and shade of perovskite solar cells. *Nat. Mater.* **2014,** *13*, 838-842.

(5) Correa-Baena, J.-P.; Abate, A.; Saliba, M.; Tress, W.; Jacobsson, J. T.; Grätzel, M.; Hagfeldt, A. The rapid evolution of highly efficient perovskite solar cells. *Energy Environ. Sci.* **2017,** *10*, 710-727.

(6) Sherahilo, T., Oxford PV perovskite solar cell achieves 28% efficiency. Oxford PV: https://www.oxfordpv.com/news/oxford-pv-perovskite-solar-cell-achieves-28-efficiency, 2018.

(7) NREL, Best Research-Cell Efficiency Chart. https://www.nrel.gov/pv/cell-efficiency.html, 2019.

(8) Lang, F.; Shargaieva, O.; Brus, V. V.; Neitzert, H. C.; Rappich, J.; Nickel, N. H. Influence of Radiation on the Properties and the Stability of Hybrid Perovskites. *Adv. Mater.* **2018,** *30*, 1702905.

(9) Deretzis, I.; Smecca, E.; Mannino, G.; La Magna, A.; Miyasaka, T.; Alberti, A. Stability and Degradation in Hybrid Perovskites: Is the Glass Half-Empty or Half-Full? *J. Phys. Chem. Lett.* **2018,** *9*, 3000-3007.

(10) Rong, Y.; Hu, Y.; Mei, A.; Tan, H.; Saidaminov, M. I.; Seok, S.; McGehee, M. D.; Sargent, E. H.; Han, H. Challenges for commercializing perovskite solar cells. *Science* **2018,** *361*.

(11) Boyd, C. C.; Cheacharoen, R.; Leijtens, T.; McGehee, M. D. Understanding Degradation Mechanisms and Improving Stability of Perovskite Photovoltaics. *Chem. Rev.* **2019,** *119*, 3418-3451.

(12) Smith, E. C.; Ellis, C. L. C.; Javaid, H.; Renna, L. A.; Liu, Y.; Russell, T. P.; Bag, M.; Venkataraman, D. Interplay between Ion Transport, Applied Bias, and Degradation under Illumination in Hybrid Perovskite p-i-n Devices. *J. Phys. Chem. C.* **2018,** *122*, 13986-13994.

(13) Nickel, N. H.; Lang, F.; Brus, V. V.; Shargaieva, O.; Rappich, J. Unraveling the Light-Induced Degradation Mechanisms of $CH_3NH_3PbI_3$ Perovskite Films. *Adv. Electron. Mater.* **2017,** *3*, 1700158.

(14) Egger, D. A.; Rappe, A. M.; Kronik, L. Hybrid Organic–Inorganic Perovskites on the Move. *Accounts Chem. Res.* **2016,** *49*, 573-581.

(15) Cao, H.; Li, J.; Dong, Z.; Su, J.; Chang, J.; Zhao, Q.; Li, Z.; Yang, L.; Yin, S. Reducing Defects in Perovskite Solar Cells with White Light Illumination-Assisted Synthesis. *ACS Energy Lett.* **2019**, 2821-2829.

(16) Khenkin, M. V.; Katz, E. A.; Abate, A.; Bardizza, G.; Berry, J. J.; Brabec, C.; Brunetti, F.; Bulović, V.; Burlingame, Q.; Di Carlo, A.; Cheacharoen, R.; Cheng, Y. B.; Colsmann, A.; Cros, S.; Domanski, K.; Dusza, M.; Fell, C. J.; Forrest, S. R.; Galagan, Y.; Di Girolamo, D.; Grätzel, M.; Hagfeldt, A.; von Hauff, E.; Hoppe, H.; Kettle, J.; Köbler, H.; Leite, M. S.; Liu, S.; Loo, Y. L.; Luther, J. M.; Ma, C. Q.; Madsen, M.; Manceau, M.; Matheron, M.; McGehee, M.; Meitzner, R.; Nazeeruddin, M. K.; Nogueira, A. F.; Odabaşi, Ç.; Osherov, A.; Park, N. G.; Reese, M. O.; De Rossi, F.; Saliba, M.; Schubert, U. S.; Snaith, H. J.; Stranks, S. D.; Tress, W.; Troshin, P. A.; Turkovic, V.; Veenstra, S.; Visoly-Fisher, I.; Walsh, A.; Watson, T.; Xie, H. B.; Yildirim, R.; Zakeeruddin, S. M.; Zhu, K.; Lira-Cantu, M. Consensus statement for stability assessment and reporting for perovskite photovoltaics based on ISOS procedures. *Nat. Energy* **2020,** *5*, 35-49.

(17) Nie, W.; Blancon, J.-C.; Neukirch, A. J.; Appavoo, K.; Tsai, H.; Chhowalla, M.; Alam, M. A.; Sfeir, M. Y.; Katan, C.; Even, J.; Tretiak, S.; Crochet, J. J.; Gupta, G.; Mohite, A. D. Light-activated photocurrent degradation and self-healing in perovskite solar cells. *Nat. Commun.* **2016,** *7*, 11574.

(18) Kwak, K.; Lim, E.; Ahn, N.; Heo, J.; Bang, K.; Kim, S.; Choi, M. An atomistic mechanism for the degradation of perovskite solar cells by trapped charge. *Nanoscale* **2019,** *11*, 11369-11378.

(19) Akbulatov, A. F.; Frolova, L. A.; Griffin, M. P.; Gearba, I. R.; Dolocan, A.; Bout, D. A.; Tsarev, S.; Katz, E. A.; Shestakov, A. F.; Stevenson, K. J.; Troshin, P. A. Effect of Electron-Transport Material on Light-Induced Degradation of Inverted Planar Junction Perovskite Solar Cells. *Adv. Energy Mater.* **2017,** *7*, 1700476.

(20) Ito, S.; Tanaka, S.; Manabe, K.; Nishino, H. Effects of Surface Blocking Layer of Sb_2S_3 on Nanocrystalline TiO_2 for $CH_3NH_3PbI_3$ Perovskite Solar Cells. *J. Phys. Chem. C.* **2014,** *118*, 16995-17000.

(21) Song, Z.; Wang, C.; Phillips, A. B.; Grice, C. R.; Zhao, D.; Yu, Y.; Chen, C.; Li, C.; Yin, X.; Ellingson, R. J.; Heben, M. J.; Yan, Y. Probing the origins of photodegradation in organic–inorganic metal halide perovskites with time-resolved mass spectrometry. *Sus. Energy Fuels.* **2018,** *2*, 2460-2467.

(22) Shlenskaya, Natalia N.; Belich, N. A.; Grätzel, M.; Goodilin, E. A.; Tarasov, A. B. Light-induced reactivity of gold and hybrid perovskite as a new possible degradation mechanism in perovskite solar cells. *J. Mater. Chem. A.* **2018,** *6*, 1780-1786.

(23) Juarez-Perez, E. J.; Ono, L. K.; Maeda, M.; Jiang, Y.; Hawash, Z.; Qi, Y. Photodecomposition and thermal decomposition in methylammonium halide lead perovskites and inferred design

principles to increase photovoltaic device stability. *J. Mater. Chem. A.* **2018,** *6*, 9604-9612.
(24) Bag, M.; Renna, L. A.; Adhikari, R. Y.; Karak, S.; Liu, F.; Lahti, P. M.; Russell, T. P.; Tuominen, M. T.; Venkataraman, D. Kinetics of Ion Transport in Perovskite Active Layers and Its Implications for Active Layer Stability. *J. Am. Chem. Soc.* **2015,** *137*, 13130-13137.
(25) Smith, E. C.; Ellis, C. L. C.; Javaid, H.; Arden, B. G.; Venkataraman, D. The use of ion-selective membranes to study cation transport in hybrid organic–inorganic perovskites. *Phys. Chem. Chem. Phys.* **2019,** *21*, 20720-20726.
(26) Domanski, K.; Roose, B.; Matsui, T.; Saliba, M.; Turren-Cruz, S.-H.; Correa-Baena, J.-P.; Carmona, C.; Richardson, G.; Foster, J. M.; Angelis, F.; Ball, J. M.; Petrozza, A.; Mine, N.; Nazeeruddin, M. K.; Tress, W.; Grätzel, M.; Steiner, U.; Hagfeldt, A.; Abate, A. Migration of cations induces reversible performance losses over day/night cycling in perovskite solar cells. *Energy Environ. Sci.* **2017,** *10*, 604-613.
(27) Hoke, E. T.; Slotcavage, D. J.; Dohner, E. R.; Bowring, A. R.; Karunadasa, H. I.; McGehee, M. D. Reversible photo-induced trap formation in mixed-halide hybrid perovskites for photovoltaics. *Chem. Sci.* **2014,** *6*, 613-617.
(28) Xing, J.; Wang, Q.; Dong, Q.; Yuan, Y.; Fang, Y.; Huang, J. Ultrafast ion migration in hybrid perovskite polycrystalline thin films under light and suppression in single crystals. *Phys. Chem. Chem. Phys.* **2016,** *18*, 30484-30490.
(29) Mosconi, E.; Angelis, F. Mobile Ions in Organohalide Perovskites: Interplay of Electronic Structure and Dynamics. *ACS Energy Lett.* **2016,** *1*, 182-188.
(30) Yuan, Y.; Huang, J. Ion Migration in Organometal Trihalide Perovskite and Its Impact on Photovoltaic Efficiency and Stability. *Accounts Chem. Res.* **2016,** *49*, 286-293.
(31) Ellis, C. L. C.; Smith, E.; Javaid, H.; Berns, G.; Venkataraman, D., Chapter 6 - Ion Migration in Hybrid Perovskites: Evolving Understanding of a Dynamic Phenomenon. In *Perovskite Photovoltaics*, Thomas, S.; Thankappan, A., Eds. Academic Press: 2018; pp 163-196.
(32) Brennan, M. C.; Ruth, A.; Kamat, P. V.; Kuno, M. Photoinduced Anion Segregation in Mixed Halide Perovskites. *Trends Chem.* **2020,** *2*, 282-301.
(33) Elmelund, T.; Seger, B.; Kuno, M.; Kamat, P. V. How Interplay between Photo and Thermal Activation Dictates Halide Ion Segregation in Mixed Halide Perovskites. *ACS Energy Lett.* **2020,** *5*, 56-63.
(34) Sun, Q.; Fassl, P.; Becker-Koch, D.; Bausch, A.; Rivkin, B.; Bai, S.; Hopkinson, P. E.; Snaith, H. J.; Vaynzof, Y. Role of Microstructure in Oxygen Induced Photodegradation of Methylammonium Lead Triiodide Perovskite Films. *Adv. Energy Mater.* **2017,** *7*, 1700977.
(35) Bryant, D.; Aristidou, N.; Pont, S.; Sanchez-Molina, I.; Chotchunangatchaval, T.; Wheeler, S.; Durrant, J. R.; Haque, S. A. Light and oxygen induced degradation limits the operational stability of methylammonium lead triiodide perovskite solar cells. *Energy Environ. Sci.* **2016,** *9*, 1655-1660.
(36) Ito, S.; Tanaka, S.; Vahlman, H.; Nishino, H.; Manabe, K.; Lund, P. Carbon-Double-Bond-Free Printed Solar Cells from TiO_2/$CH_3NH_3PbI_3$/CuSCN/Au: Structural Control and Photoaging Effects. *ChemPhysChem* **2014,** *15*, 1194-1200.
(37) Boote, B. W.; Andaraarachchi, H. P.; Rosales, B. A.; Blome-Fernandez, R.; Zhu, F.; Reichert, M. D.; Santra, K.; Li, J. Z.; Petrich, J. W.; Vela, J.; Smith, E. A. Unveiling the Photo- and Thermal-Stability of Cesium Lead Halide Perovskite Nanocrystals. *ChemPhysChem* **2019,** *20*, 2647-2656.
(38) Charles, B.; Dillon, J.; Weber, O. J.; Islam, M. S.; Weller, M. T. Understanding the stability of mixed A-cation lead iodide perovskites. *J. Mater. Chem. A.* **2017,** *5*, 22495-22499.
(39) Zhang, Y.; Grancini, G.; Feng, Y.; Asiri, A. M.; Nazeeruddin, M. K. Optimization of Stable Quasi-Cubic $FA_xMA_{1-x}PbI_3$ Perovskite Structure for Solar Cells with Efficiency beyond 20%. *ACS Energy Lett.* **2017,** *2*, 802-806.
(40) Binek, A.; Hanusch, F. C.; Docampo, P.; Bein, T. Stabilization of the Trigonal High-Temperature Phase of Formamidinium Lead Iodide. *J. Phys. Chem. Lett.* **2015,** *6*, 1249-1253.
(41) Kieslich, G.; Sun, S.; Cheetham, A. K. Solid-state principles applied to organic–inorganic perovskites: new tricks for an old dog. *Chem. Sci.* **2014,** *5*, 4712-4715.
(42) Ke, W. J.; Stoumpos, C. C.; Zhu, M. H.; Mao, L. L.; Spanopoulos, I.; Liu, J.; Kontsevoi, O. Y.; Chen, M.; Sarma, D.; Zhang, Y. B.; Wasielewski, M. R.; Kanatzidis, M. G. Enhanced photovoltaic performance and stability with a new type of hollow 3D perovskite {en}$FASnI_3$. *Sci. Adv.* **2017,** *3*, 9.
(43) Spanopoulos, I.; Ke, W. J.; Stoumpos, C. C.; Schueller, E. C.; Kontsevoi, O. Y.; Seshadri, R.; Kanatzidis, M. G. Unraveling the Chemical Nature of the 3D "Hollow" Hybrid Halide Perovskites. *J. Am. Chem. Soc.* **2018,** *140*, 5728-5742.
(44) Węcławik, M.; Gągor, A.; Piecha, A.; Jakubas, R.; Medycki, W. Synthesis, crystal structure and phase transitions of a series of imidazolium iodides. *CrystEngComm* **2013,** *15*, 5633-5640.
(45) Hartono, N. T. P.; Sun, S.; Gélvez-Rueda, M. C.; Pierone, P. J.; Erodici, M. P.; Yoo, J.; Wei, F.; Bawendi, M.; Grozema, F. C.; Sher, M.-j.; Buonassisi, T.; Correa-Baena, J.-P. The effect of structural dimensionality on carrier mobility in lead-halide perovskites. *J. Mater. Chem. A.* **2019,** *7*, 23949-23957.
(46) Daub, M.; Haber, C.; Hillebrecht, H. Synthesis, Crystal Structures, Optical Properties, and Phase Transitions of the Layered Guanidinium-Based Hybrid Perovskites $[C(NH_2)_3]_2MI_4$; M = Sn, Pb. *Eur. J. Inorg. Chem.* **2017,** *2017*, 1120-1126.
(47) Szafrański, M.; Katrusiak, A. Phase transitions in the layered structure of diguanidinium tetraiodoplumbate. *Phys. Rev. B.* **2000,** *61*, 1026-1035.
(48) Wilke, M.; Casati, N. Insight into the Mechanochemical Synthesis and Structural Evolution of Hybrid Organic–Inorganic Guanidinium Lead(II) Iodides. *Chem. Eur. J.* **2018,** *24*, 17701-17711.
(49) Brown, M. E. The Prout-Tompkins rate equation in solid-state kinetics. *Thermochim. Acta* **1997,** *300*, 93-106.
(50) Brown, M. E.; Glass, B. D. Pharmaceutical applications of the Prout–Tompkins rate equation. *Int. J. Pharm.* **1999,** *190*, 129-137.
(51) Prout, E. G.; Tompkins, F. C. The thermal decomposition of potassium permanganate. *Trans. Farad. Soc.* **1944,** *40*, 488-498.
(52) Giorgi, G.; Fujisawa, J.-I.; Segawa, H.; Yamashita, K. Organic–Inorganic Hybrid Lead Iodide Perovskite Featuring Zero Dipole Moment Guanidinium Cations: A Theoretical Analysis. *J. Phys. Chem. C.* **2015,** *119*, 4694-4701.
(53) Pandey, S. K.; Manogaran, D.; Manogaran, S.; Schaefer, H. F. Quantification of Hydrogen Bond Strength Based on Interaction Coordinates: A New Approach. *J. Phys. Chem. A* **2017,** *121*, 6090-6103.
(54) Fu, Y. P.; Hautzinger, M. P.; Luo, Z. Y.; Wang, F. F.; Pan, D. X.; Aristov, M. M.; Guzei, I. A.; Pan, A. L.; Zhu, X. Y.; Jin, S. Incorporating Large A Cations into Lead Iodide Perovskite Cages: Relaxed Goldschmidt Tolerance Factor and Impact on Exciton-Phonon Interaction. *ACS Central Sci.* **2019,** *5*, 1377-1386.
(55) Jodlowski, A. D.; Roldan-Carmona, C.; Grancini, G.; Salado, M.; Ralaiarisoa, M.; Ahmad, S.; Koch, N.; Camacho, L.; de Miguel, G.; Nazeeruddin, M. K. Large guanidinium cation mixed with methylammonium in lead iodide perovskites for 19% efficient solar cells. *Nat. Energy* **2017,** *2*, 972-979.
(56) Yun, J. S.; Seidel, J.; Kim, J.; Soufiani, A.; Huang, S.; Lau, J.; Jeon, N.; Seok, S.; Green, M. A.; Ho-Baillie, A. Critical Role of Grain Boundaries for Ion Migration in Formamidinium and Methylammonium Lead Halide Perovskite Solar Cells. *Adv. Energy Mater.* **2016,** *6*, 1600330.
(57) Pont, S.; Bryant, D.; Lin, C.-T.; Aristidou, N.; Wheeler, S.; Ma, X.; Godin, R.; Haque, S. A.; Durrant, J. R. Tuning

$CH_3NH_3Pb(I_{1-x}Br_x)_3$ perovskite oxygen stability in thin films and solar cells. *J. Mater. Chem. A.* **2017,** *5*, 9553-9560.

(58) Kim, G. Y.; Senocrate, A.; Yang, T.-Y.; Gregori, G.; Grätzel, M.; Maier, J. Large tunable photoeffect on ion conduction in halide perovskites and implications for photodecomposition. *Nat. Mater.* **2018,** *17*, 445-449.

(59) Juarez-Perez, E. J.; Hawash, Z.; Raga, S. R.; Ono, L. K.; Qi, Y. Thermal degradation of $CH_3NH_3PbI_3$ perovskite into NH_3 and CH_3I gases observed by coupled thermogravimetry–mass spectrometry analysis. *Energy Environ. Sci.* **2016,** *9*, 3406-3410.

(60) Motti, S. G.; Meggiolaro, D.; Barker, A. J.; Mosconi, E.; Perini, C. A. R.; Ball, J. M.; Gandini, M.; Kim, M.; De Angelis, F.; Petrozza, A. Controlling competing photochemical reactions stabilizes perovskite solar cells. *Nat. Photon.* **2019,** *13*, 532-539.

(61) Wang, S.; Jiang, Y.; Juarez-Perez, Emilio J.; Ono, Luis K.; Qi, Y. Accelerated degradation of methylammonium lead iodide perovskites induced by exposure to iodine vapour. *Nat. Energy* **2016,** *2*, 16195.

(62) Fu, F.; Pisoni, S.; Jeangros, Q.; Sastre-Pellicer, J.; Kawecki, M.; Paracchino, A.; Moser, T.; Werner, J.; Andres, C.; Duchêne, L.; Fiala, P.; Rawlence, M.; Nicolay, S.; Ballif, C.; Tiwari, A. N.; Buecheler, S. I_2 vapor-induced degradation of formamidinium lead iodide based perovskite solar cells under heat–light soaking conditions. *Energy Environ. Sci.* **2019,** *12*, 3074-3088.

For Table of Contents Only

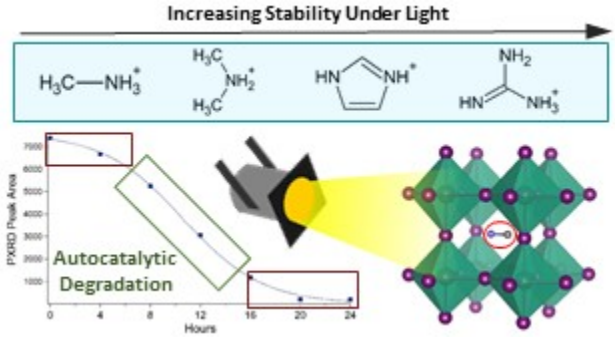

Hybrid organic-inorganic perovskite materials where the prototypical methylammonium cation was substituted for varying percentages of larger organic cations (imidazolium, guanidinium, and dimethylammonium) were synthesized. These new materials exhibited increased stability under light, with degradation rates up to 62% slower. When degraded under light, the materials revealed a unique autocatalytic degradation mechanism. The results show that substitution of these larger cations could be a promising strategy for designing more light-stable hybrid perovskite materials